Urban Drainage Decision Model for Storm Emergency Management Based on Multi-objective Optimization

Shitai Bao
Augur Intelligent Technology Co. Ltd
Zehui Lai
Augur Intelligent Technology Co. Ltd
Biao Chen
Augur Intelligent Technology Co. Ltd
Shunqing Chen (chensq@augurit.com)
Augur Intelligent Technology co., LTD

Research Article

Keywords: Urban water-logging, Surface water simulation, Cellular automata, Drainage optimization modeling, Multi-objective optimization

Posted Date: May 16th, 2022

DOI: https://doi.org/10.21203/rs.3.rs-1607481/v1

Urban Drainage Decision Model for Storm Emergency Management Based on Multi-objective Optimization

Shitai Bao[1], Zehui Lai[2], Biao Chen[2], Shunqing Chen[2*]

[1] College of Resource and Environment, South China Agricultural University, Guangzhou, 510642, China

[2] Center of R&D, Augur Intelligent Technology Co., Ltd, Guangzhou 510663, China

***Corresponding author**: chensq@augurit.com

Acknowledgments

The authors wish to thank the Drainage Facilities Management Center in Guangzhou for providing the spatial data and water-log observation data. This research was partially supported by a grant from Guangzhou Major Sci-Tech project award no. 202103050001 in China.

Abstract: Urban water-logging is a challenging environmental issue in most urban areas. Effective, process-oriented water-logging simulation and drainage optimization models have become imperative for urban storm water and emergency management. This research provides a solution to urban water-logging through integrating water-logging prediction and drainage optimization schemes based on theories of cellular automaton and multi-objective optimization. An urban water-logging model for uncertain flow is constructed by using cellular automaton and rules in consideration of urban surface fragmentation and space complexity instead of definite mathematical equations. For dynamic simulation, outputs of water depth and flooded areas are projected with inputs of rainfall, soil infiltration, plant interception, gully discharge, and outflow to its neighbors in each cell, at any moment. The drainage decision model for optimal solutions is designed to calculate the maximal amount of water to be pumped from flooded zones to candidate reservoirs with minimal energy cost by using a multi-objective optimization approach. This integrated approach was successfully applied in the DongHaoChong catchment (11 km^2) watershed, a central urban area of Guangzhou, southern China, to forecast urban water-logging and optimize drainage decision-making. The results shows that the simulation model in this study is reliable as a whole and is capable of simulating uncertain flow at any position at any moment with minimal data input and parameters in an urban environment. An integrated solution to urban water-logging prediction and drainage optimization can optimize decision-making to alleviate urban water-logging.

Keyword: Urban water-logging; Surface water simulation; Cellular automata; Drainage optimization modeling; Multi-objective optimization

1. Introduction

In recent decades, urban water-logging has become a challenging environmental issue in most urban areas of most developing countries, often resulting in serious disasters, such as traffic breakdown, property loss, and even loss of life. Urban water-logging is largely influenced by climate change and rapid urbanization and is likely to occur when climate extremes with torrential rain, heavy rainfall, and continuous precipitation become more frequent, resulting in the urban drainage capacity being exceeded (Gu and Gu 2014). Urban water-logging is intensified by rapid urbanization with increased impervious surfaces, insufficient construction, or maintenance of drainage systems, and a laggard civil engineering management system (Valipour 2014). Hence, an urgent need exists to develop functional tools for efficient decision-making to improve urban storm water management and utilization for water-logging prevention (Asia Development Bank 2014).

Model-based simulation and prediction is an effective, and low-impact development (LID), measure to reduce adverse hydrologic effects of urban storm-water (Elliott and Trowsdale 2007). Hydraulic modeling is an important element for establishing a robust flood forecasting framework. Simulation results from hydraulic models can be used to generate inundation maps to evaluate flood risk. Indeed, various models have been developed to address water flow within canals and rivers. These models evolved from simple, empirical hydrology descriptions into incredibly complex models based on

62 discretized, numerical solutions of general laws (Parsons and Fonstad 2007). Generally,
63 numerical simulations require certain assumptions in the governing equations. Simple
64 hydraulic modeling approaches may be good for estimating flood propagation. However,
65 the effects of infrastructure or complex overland flow typically need to be considered for
66 complicated hydraulic investigation. For example, the U.S. Geological Survey (USGS)
67 developed a one-dimensional river flow and water quality model (Spitz 2007) into a two-
68 dimensional model for hydraulic processes requiring detailed hydraulic information.
69 Traditional equations of continuity and motion were used to simulate approximate water-
70 log depth on overland surfaces (Dong and Lu 2008). The Soil Conservation Service (SCS)
71 model was utilized to simulate urban surface runoff depth and assess water-log (Quan et
72 al. 2010). Moreover, diffusive-wave approximation of the Saint-Venant equations was
73 developed to simulate surface water by integrating the USGS modular flow model
74 (Hughes et al. 2014).

75 These previous studies can be regarded as successful applications in numerical
76 simulations of surface water systems, and provide a useful means to understand and
77 predict regional hydrology processes in a natural environment. However, it is somewhat
78 difficult to describe stochastic and uncertain surface flow in relatively small temporal and
79 spatial scales in urbanized areas. The urban area differs from natural areas in its high
80 fragmentation of land cover and densely distributed civil buildings and infrastructure.
81 However, a cellular automaton (CA) model, a self-organization approach, provides an
82 efficient alternative to physical-based models for simulating complicated hydrologic
83 processes. The CA model with simple local interaction rules has been successfully applied

84 in water flow simulations (Cirbus and Podhoranyi 2013; Ma et al. 2009). For example,
85 Parsons and Fonstad (2007) coupled the conservation of mass and Manning's equations
86 with an algorithm to slow down the movement of water flow from one pixel to the next
87 until the correct timing was achieved. Ma et al. (2009) developed a novel, quantitative
88 automaton model that projected hillslope runoff and soil erosion caused by rainfall events.
89 Cirbus and Podhoranyi (2013) simulated the spreading of liquid using a CA and
90 comparatively simple rules and conditions, which included several factors. Liu et al.
91 (2014) developed a two-dimensional CA model using Von Neumann neighborhood to
92 simulate flood inundation on urban roads. These applications suggest that a CA model is
93 feasible and has significant potential to simulate uncertain water flow in urban areas.
94 Despite progress in sustainable urban water management, it remains imperative to
95 develop efficient decision support systems to reduce costs for urban storm water
96 management (Bach et al. 2014; Ellis et al. 2004; Marlow et al. 2013). Although
97 investigation of multi-objective issues in water resources have received considerable
98 attention in large basins and for predicting flooding events in cities, less attention has been
99 focused on urban drainage decisions (Labadie et al. 2012; Park et al. 2012; Penn et al.
100 2013; Wang et al. 2013; Woodward et al. 2014). As such, the primary purpose of this study
101 is to provide a solution to urban waterlogging through the integration of waterlogging
102 predictions and drainage optimization schemes based on theories of cellular automata and
103 multi-objective optimization. The findings of the study will provide an effective way to
104 improve drainage decision-making and emergency response measures based on existing
105 conditions. More specifically, if urban waterlogging can be accurately simulated according

106 to the rainfall forecast and urban situations, potential flooded areas can be predicted. In the
107 current study, an urban waterlogging simulation model was constructed using cellular
108 automaton and rules in place of definite mathematical equations. The outputs of this model
109 include uncertain flow and water depth at random places and times, with required inputs of
110 rainfall precipitation, digital elevation model (DEM), land use cover, and drainage gully
111 geometry. A drainage decision model supported by multi-objective optimization is then
112 proposed to pump water from flooded zones to candidate reservoirs. The emergency
113 response based on optimal drainage decisions for stakeholders is then determined in
114 advance and water is transported from flooded areas into candidate reservoirs, thereby
115 decreasing the negative impacts of water-logging and property loss. Collectively, an
116 integrated solution is proposed to use the input simulation results to dynamically compute
117 numerous optimal drainage schemes for decision-makers using genetic algorithms. This
118 optimal solution to urban waterlogging prediction and drainage decisions was applied in
119 the DongHaoChong catchment, in the central urban area of Guangzhou, China, after being
120 calibrated and validated. In this way, we were able to validate the prediction of
121 waterlogging based on an accurate simulation of uncertain flow on urban ground, and to
122 optimize the drainage solutions for emergency decision-making.
123

124 **2. Methodology**

125 **2.1 Water-log simulation model**

126 An urban water-log model was designed based on a regular cellular automata (CA)
127 model by simplifying the computation of the hydrology process with a grid-based

simulation frame. The cells of the CA were defined as a square grid filling a two-dimensional (2D) space, which is in accordance with the grid cell of raster data covering the whole study area. The Moore neighborhood was used, comprising eight directions (*D8*) surrounding the central cell (Cirbus and Podhoranyi 2013). The status sets were divided into static status and dynamic status in computation of the central cell. The static status of the current cell retained values of height *H(c)*, sink reservoir *S(c*), and plant interception *I(c*). The dynamic status included rainfall *r(c,t)*, soil infiltration *sI(c,t)*, outflow *o(c,t)*, gully discharge *g(c,t)*, and water depth *h(c,t)*. The next status of the central cell depended on the current status of the adjacent eight neighbors and its own status, according to the CA regulation. Transition rules and regulations mainly determine the direction and depth of surface flow between the central cell and adjacent cells. The regulation can be expressed as follows in Equations (1) and (2):

$$[h(c,t-1),\Delta h] \overset{R}{\rightarrow} h(c,t) \tag{1}$$

$$\Delta h = r(c,t) - S(c) - I(c) - sI(c,t) - g(c,t) - o(c,t) + \sum_1^8 o(B,t) \tag{2}$$

where Δh is the change of inundated water depth in the central cell at current time t since previous time *h(c, t-1)*; *o(B,t* represents the potential outflow from its eight neighbors to the central cell at time t while its neighbors individually become the central cell; and *o(c, t)* denotes probable outflow from the central cell to its neighbors.

The production of runoff depends on the kind of urban ground surface during a storm. According to the difference in runoff production, the urban surface is divided into permeable (green land, lake, river, railway) and impermeable surfaces (building, road, square, viaduct). Three assumptions are applied in this model: (1) If the cell is covered by

150 an impervious surface, both soil infiltration *sI(c)* and plant interception *I(c)* always equal
151 zero; (2) Water on cells covered by buildings or viaducts are fully collected by the sewer
152 system, so these cells are never inundated and their water depth always equals zero; (3) If
153 no gully is in the current cell, the cell's outflow from the drainage system is always zero.
154 The calculation of water depth therefore depends on different surfaces (Table 1).

155 Here, rainfall *r(c,t)* is assigned values (mm/min) from the observed data or the
156 estimated data. Both the sink reservoir, S(c), and plant interception, I(c), are constants and
157 depend on empirical values with different surfaces or parameters determined using
158 repeated experiments. The soil infiltration loss, *sI(c,t),* is calculated using Horton's
159 equation (Equation 3) (Ma et al. 2009):

160 $$sI(c,t) = \left[f_c + (f_0 - f_c)e^{-\lambda t}\right]\Delta t/60 \quad (3)$$

161 where f(t) is the infiltration rate (mm per min) at time t (min); f_c and f_0 are the stable and
162 initial infiltration rates (mm per min), respectively; Δt is the iteration interval (ms); and λ
163 is a constant. The *g(c,t)* of gully discharge is calculated using the hydraulics equation
164 (Equation 4) (Gao 2006)：

165 $$g(c,t) = W * C * k * \Delta t * \sqrt{2g * \frac{h(c,t)}{1000}}/S \quad (4)$$

166 where W is the surface area of the drainage gully in the current cell (m^2), C is the flow
167 coefficient of the gully, and K is the blocking coefficient of the gully. S is the surface area
168 of the current cell (m^2), h(c,t) is the previous depth of the current cell before the gully
169 discharges (mm), and *g* is the gravitational acceleration constant (9.81 m/s^2).

170 After considering sink reservoirs, plant interception, soil infiltration, and gully
171 discharge, the rest of the storm water may produce surface flow of uncertain direction and

velocity. The distribution flow between the central cell and its neighbors is the key to cellular regulation. Usually it assumes that direction of slow flow is determined mainly by gravity in laminar flow, which can be judged by the Reynolds number (Ma et al. 2009). The laminar flow occurs from the central cell to one of the adjacent cells uncovered by buildings with the steepest descent or maximum drop. If there are more than two of the same maximum drops in laminar flow, the water randomly flows onto one of its neighbors with the same maximum drop. An empirical Manning's equation can be used in CA to calculate the flow velocity (Cirbus and Podhoranyi 2013; Liuet al. 2014; Ma et al. 2009). The flow velocity directly influences intervals, Δt(s), of the simulation iterations, which should approximate the minimal time of flow through the current cell in the whole grid space. Then, the amount o(c,t) of interchanged water in time Δt(s) from the central cell to one neighborhood is formulated using Equation (5):

$$o = VS'\Delta t/S = \frac{(h^{2/3} j^{1/2}/n')*(h*L)*\Delta t}{(L*L)} = h^{5/3} j^{1/2} \Delta t/(L * n') \quad (5)$$

where V (m s^{-1}) is the flow velocity, depending on the water depth of the current cell (h), its water surface slope (j), and Manning's roughness coefficient on its cover (n'). S' (m^2) is the area of the flow side from the central cell to its neighbor with maximum drop, S (m^2) is the surface area of the central cell, and L is the length of the cellular side (m). Water surface slope, j, is computed by using the slope algorithm of Burrough and McDonnell (1998).

However, the Manning formula diverges from supposed optimal conditions (Diaz 2005), while the flow becomes turbulent with higher velocity and depth, and viscous forces have little effect. The accuracy of the Manning formula is lacking at a larger

194 Reynolds number, which indicates that the fluid undergoes irregular fluctuations or mixing
195 when fully turbulent (Engineeringtoolbox 2015). In turbulent flow, the speed of the fluid at
196 a point is continuously undergoing changes in both magnitude and direction, replacing the
197 steady direction from the central cell to its one neighbor with maximum drop in laminar
198 flow. Liu et al. (2014) distributed water from a central cell to its four neighbors in their CA
199 model based on an algorithm that aims to minimize the water surface elevation difference
200 between cells regardless of whether the flow is laminar or turbulent, however, this ignores
201 a violation instance of the central cell with a high elevation and low water depth. In the
202 current study, an improved algorithm is proposed to calculate a minimal water surface
203 elevation during an iteration time between the current cell and its neighbors with low
204 water surface in turbulent flow. The core of the improved algorithm is to minimize the
205 water surface elevation $ave(t')$ after distribution of the water from the central cell to
206 adjacent cells uncovered by buildings with low water surface (Equation (6)):

207 $$ave(t') = \frac{1}{k}\left(\sum_{i=1}^{l\in S} Depth(i,t) + \sum_{j=1}^{k\in S} Dem(j)\right) \quad (6)$$

208 where l is the amounts of set (S), including the central cell and its neighbors with lower
209 elevation; k is variable and depends on the elevation, which is not less than $ave(t')$. If
210 elevations of those cells are greater than $ave(t')$, k equals l and water depth of all cells is
211 $ave(t')$. Otherwise, water depth on the cell with elevation higher than the average water
212 surface elevation equals zero or a minuscule number, and k individually decreases until
213 $ave(t')$ is greater than the highest elevation in the remaining cells.

214

215 **2.2 Drainage optimization model**

Among many measures employed for drainage emergency, forced drainage by pumping is an efficient measure. When all flood water is pumped from the selected water-logged areas to candidate reservoirs, drainage decisions should consider certain optimization problems. How to maximize pumping volume and minimize energy cost are the basic concerns. A practical optimization model is proposed using specific variables:

x_i: index of flooded area, I, from 0 to I, I depends on the simulation results of the water-log model

j: index of candidate reservoirs, j, from 1 to J, J is a constant

V_i: original volume of the flooded area, i, unit is cubic meters

C_j: maximal capacity volume that potential reservoir, j, can bear of the flood water without danger, which is a given value; its unit is cubic meters

A_{ij}: distance of the cost path to transfer the flood from area i to reservoir j, which depends on the distance and slope between flooded area i and reservoir j, unit is meters

$$A_{ij} = sqrt((c\,ellsize * (row_i - row_j))^2 + (c\,ellsize * (col_i - col_j)^2) + (H_j - H_i)^3)$$

H_i: height of the deepest place in flooded area, i,

H_j: height of the deepest point in reservoir, j.

Using the cube of the height difference not only shows the contribution of height difference, but also represents the influence of it being downstream or upstream.

g: gravitational acceleration constant

ρ: density of water, a given value

x_{ij}: binary decision variant indicating whether the flooded area i, is transferred to reservoir j; if it equals 1, then all of the flood at area i, is transferred to the reservoir j; otherwise, it equals 0.

Objective function:

$$Outflood: max \sum_{i=0}^{I} V_i \sum_{j}^{J} x_{ij} \quad (7)$$

$$PowerCost: min \quad \frac{\rho * g}{360 \sum_{i=0}^{I} V_i \sum_{j=1}^{J} A_{ij} * x_{ij}} \quad (8)$$

subject to

$$\sum_{i}^{I} x_{ij} V_i \leq C_j \quad \forall j \quad (9)$$

$$\sum_{j=1}^{J} x_{ij} \leq 1 \quad \forall i \quad (10)$$

$$x_{ij} \in \{0,1\} \quad (11)$$

Objective (7) seeks to maximize volume of the transferred flood (unit: cubic meters).

Objective (8) seeks to minimize the power cost of transferring the flood (unit: kWh). Here, cost is the product of transferring volume (cubic meter), distance (meter), density (1020 kg per cubic meter), and acceleration of gravity (9.81 kg per square second).

Constraint (9) ensures that the total transferred flood does not exceed the maximal capacity of every reservoir.

Constraint (10) indicates that one flooded area can only transfer to one reservoir.

Constraint (11) specifies binary restrictions on variables.

Many algorithms can be applied to resolve such multi-objective optimization issues. An important feature in multi-objective optimization is to find a diverse set of optimal solutions for the problem so that the Pareto front can be approximated. Recent studies in the optimization literature have demonstrated the effectiveness of genetic algorithms

(GAs) in solving multi-objective problems. GAs is one of the most promising techniques and have received wide attention due to their flexibility and effectiveness in optimizing complex systems. Here, the *gamultiobj* algorithm used in Matlab2014 is a controlled elitist genetic algorithm, a variant of NSGAII. An elitist GA always favors individuals with a better fitness value (MathWorks 2012). For additional details regarding the use of GAs in solving multi-objective optimization problems, we refer the reader to relevant literature (Deb 2001; GarcíarPalomares et al. 2012; Liu et al. 2005; Samanlioglu 2013; Xiao et al. 2007).

3. Application of models

3. 1 Study area and datasets

DongHaoChong catchment with an area of 11 km^2 is in the central urban area of Guangzhou. The DongHaoChong canal is a main branch of the Pearl River, with full length of 4,225 meters and a width of 7–11 m. It originates in Luhu Lake in the south of the Baiyun Mountain, and its elevation in the catchment decreases from north to south (Fig. 1). The river flows through an old urban area of Guangzhou from north to south, with part of a closed conduit. Big flooding has occurred for decades, and flooding risk has been intensified in rainstorms in recent years due to increased building density and old drainage infrastructure.

The data primarily comprise spatial data related to the CA model (Table 2). All source data was obtained from the Drainage Facilities Management Center in Guangzhou, including DEM, green land, buildings, roads, reservoirs, lakes, rivers, drain gullies, and

282 rainfall. The resolution of the original DEM data is 5 m. The cellular space was built in
283 accordance with DEM in the study area and is divided into 790,860 square grids in 980
284 columns and 807 rows of 5 m width. The land use layer is composed of the green land,
285 building, road, river, and lake, in which (1) represents road, (2), building, (3), green land,
286 and (4) is a river or lake. The land use layer is converted into raster data and snapped to
287 the DEM data with 5 m resolution. The gully is a part of the sewer system in the urban
288 environment, usually present along the road edges. Gully data is a geographic point vector,
289 with a geometry point location and certain attributes, including surface size and a block
290 coefficient. In the CA model, gully data can be transferred into three grid layers of surface
291 size (m^2), flow, and block coefficient, explicitly represented by individual pixels. The
292 rainfall is time series data from observation or prediction, assuming that the rain is well-
293 distributed at a small scale.
294
295 **3.2 Simulation, calibration, and validation**
296 Based on the described two models, a workflow of computation was developed using
297 Matlab2014 (Fig. 2). First, the rainfall and spatial data listed in Table 2 were processed
298 into arrays, then cells and parameters were initialized. According to the simulation
299 duration and initial iteration interval, the number of iterations was calculated and the
300 iterations began. With the change in x and y in the circular body of the cellular array, every
301 current cell became a central cell and was first judged by its cover type. If its cover was
302 not building and 'no data,' its current water depth H(c,t) was computed according to
303 regulations (2) and (3), including computing soil infiltration sI(c,t), gully discharge g(c,t),

304 and outflow to its neighbor, o(c,t). Based on the velocity of outflow from the central cell to
305 its neighbor with a positive maximal drop, the iteration interval was refined by comparing
306 the time of flow from the central cell to its orthogonal or diagonal cell. If the iteration
307 interval was less than the minimal time of outflow from the central cell to its neighbor, the
308 depth of outflow was calculated and added into the neighbor. Otherwise, a new process
309 was recomputed according to the new iteration interval. The Reynolds number was
310 calculated to judge whether outflow is fully turbulent. If the flow was turbulent, the
311 improved algorithm that minimizes the lowest water surface was used to distribute water
312 to the adjacent nine cells. Water depth in every cell was updated at every iteration. The
313 iteration amount was determined by dividing the simulation time (minutes) by the iteration
314 interval (seconds), which did not cause a significant increase in the computational
315 complexity. After all iterations, water-log depth grids at all times were ready and a grid at
316 any time point could be output in raster format.

317 Two recent representative rainstorm-flooding events were selected to calibrate and
318 validate the proposed model. These two rainstorms (August 15, 2013 and June 23, 2014)
319 resulted in severely water-logged areas. The rainstorm of August 15, 2013 had a rainfall
320 precipitation of 122.7 mm (with 78.5 mm at the first 5 h, 14 h of the total) and inundated
321 half of the study area. Meanwhile, that on June 23, 2014 had a rainfall precipitation of 96
322 mm (lasting 3 h of the total), resulting in obvious inundation.

323 The simulated results coincided well with the observed water-log in the study area.
324 Certain main water-log areas, which are usually located near roads, were observed and
325 reported by the Center of Drainage Facility Management in Guangzhou. Thirteen flooded

326 points from August 15, 2013, and 23 points from June 23, 2014 were observed (Fig. 3a).
327 The root mean standard error (RMSE) values—calculated by comparing the predicted
328 depth with the observation—were 26.89 mm and 78.48 mm in 2013 and 2014,
329 respectively. A total of 23 points were reported on June 23, 2014 compared with the
330 simulated depth to yield the RMSE. Water-log was heavier on 23 June than on 15 August,
331 as the storm on 23 June was heavier in rainfall intensity and precipitation. The prediction
332 at certain flooded areas was higher than the observation on 23 June, caused by hysteretic
333 measurement of those flooded areas. Moreover, the deviation of the 23 June prediction
334 was larger than that for 15 August, which may be influenced by several factors and will be
335 discussed later. As a whole, the results state the simulation is precise and valid (Figs 3a
336 and 3b).
337 Through the validation of the simulation results, some parameters were further
338 calibrated and updated (Table 3). The values of parameters were revised to minimize the
339 deviation between observations and simulation results, most of which were initialized and
340 evaluated based on empirical values (Fuping et al. 2010; Schaffranek 2004; Valipour
341 2014).
342
343 **3.3 Water-log prediction**
344 To reduce the loss of urban water-log and improve emergency levels of drainage
345 management, water depth on urban surfaces was simulated with given rainfalls based on
346 the above models. The study area is supposed to encounter 1-year, 10-year, 50-year, 100-
347 year storms, which refers to total rainfalls that have a one percent probability of occurring

348 at that location in that year. According to the central urban rainstorm formula and
349 calculation chart in Guangzhou city (Water Affairs Bureau 2011), the rainfall amount of
350 the 100-year storm is 115 mm in one hour, the 50-year storm is 106 mm, the 10-year storm
351 is 85 mm, and the 1-year storm is 55 mm. With the rainfall gross, the rainfall per minute
352 can be simulated based on rainstorm intensity.

353 Running the simulation model, a three-dimensional matrix (980,807,60) of water
354 depth in the study area was generated for 60 minutes of the 100-year rainfall. The array at
355 random times can be chosen as the result of simulation, and as a template to create a new
356 zero matrix for marking flooded areas. First, the deepest cell was searched in the result
357 array and the value of the corresponding cell was updated to the ID of the flooded area in
358 the marked array. Using the searching method with a 3 × 3 window, all neighbors with
359 values greater than the water-log tolerance (50 mm) were found and corresponding cells
360 were marked with the same ID as the deepest cell. The second deepest cell was then
361 searched at unmarked positions in the result array. Its neighbors were searched and their
362 corresponding positions were marked with the same ID as in the marked array. Similarly,
363 the rest of the marked array was updated with the IDs and water-log areas were predicted.
364 More detailed information was extracted and recorded, such as sum flood volume and
365 area, depth, height, and the row and column of the deepest cell in every water-log area.
366 Similarly, the water-log was predicted by inputting the amounts of 50-year storm, 10-year
367 storm, and 1-year storm.

368 The predicted water-log is useful to make drainage decisions and take emergency
369 measures by pumping the flood water to reservoirs to avoid life and property loss. As a

370 measure of low impact development (LID), forced drainage by pumping is currently one
371 of most popular emergency measures in many Chinese cities. The drainage solutions
372 should meet the maximum pumping volume with the minimum energy cost. Based on the
373 above drainage optimization model, it was simple to design numerous optimal drainage
374 decisions.
375
376 **4 Results and discussion**
377 **4.1 Prediction results and accuracy**
378 The predicted water-log with different storms is shown in Fig. 4. With the fall amount
379 increasing, the area and depth of water-log gradually rise. According to 100-year rainfall
380 forecast in the study area, the heaviest water-log areas with a volume above 50 cubic
381 meters and a depth beyond 150 mm are filtered. Sixty heavy flood areas and eight
382 reservoirs are shown on the map (Fig. 5). There are nine water-logged areas around Luhu
383 Lake influenced by the undulating terrain, with many marshlands. Other water-logged
384 areas are mainly located near roads with few gullies; few are on green land.
385 The simulation model in this study is reliable overall, however the accuracy of the CA
386 model needs refinement. The accuracy of simulation depends on many factors, including
387 the basic data and simulation parameters. First, the precision of basic data directly
388 influences the accuracy of flow simulation, such as refinement of land use and resolution
389 of DEM and cells. Second, precision of the parameters listed in Table 3 has a
390 comprehensive impact on simulation accuracy. Certain empirical parameters, e.g., Horton
391 equation parameters and the Manning coefficient, can be calibrated gradually to coincide

392 with real conditions related to ground runoff and inundation in the urban environment.
393 Recent research indicates the Manning coefficient at the same patch during the storm may
394 not be constant due to a decrease in the relative roughness, for example, greater depth,
395 increased slope, or turbulent flow velocity. It is therefore necessary to check the status of
396 flow using the Reynolds number or other formulas. Iteration interval has a unique
397 influence on simulation and may result in accumulated errors in a long simulation
398 duration, such as the larger deviation observed on 23 June 2014 (Fig. 3). In this study, the
399 setting of the iteration interval(s) was close to the minimal time of the water flow from the
400 cell center to its adjacent cell with the velocity calculated using Manning equation.
401 Storm sewer surcharge is not considered in the model and it is assumed that the storm
402 sewerage system fully functions during a storm event. The static block coefficient of the
403 gully should be dynamic to generate a more accurate contribution to the simulation.
404 Finally, the complexity of the CA model must be improved. Facing sophisticated urban
405 hydrologic environments, outflow is synchronized with other factors of soil infiltration and
406 gully discharge. However, the quantitative influences of those factors are calculated in the
407 CA model, which may result in implicit deviation due to lack parallel computation
408 between those factors. Furthermore, a potential reciprocal effect is not considered in the
409 CA model.
410
411 **4.2 Optimization results and improvement**
412 Considering the sewer surcharge, the water-log may be heavier during the 100-year
413 storm, which causes severe threat of loss of property and life. By running the optimization

414 program, optimal drainage solutions were obtained. Since the bi-objective model has
415 multiple objectives, it often has many optimal solutions. For example, let us consider an
416 optimal solution to such a problem that has a volume of v1 and cost of c1. There may exist
417 another solution with a lower volume of v2 < v1, but a cost of c2, which is less than c1.
418 Since neither option is inherently better than the other, they are both considered optimal or
419 none dominate. The set of all optimal solutions to the problem together is called the Pareto
420 front, representing the trade-offs between the two objectives (Fig. 6).

421 To assess the optimization solutions, a weighted sum method was selected, which
422 applies a set of weights to the objectives so that they are converted into a single objective.
423 Hence, two objectives are combined in Equations (7) and (8) into one objective, as
424 follows:

425 $$max: w \sum_{i=0}^{I} V_i \sum_{j}^{J} x_{ij} - (1-w)\, \rho g \sum_{i=0}^{I} V_i \sum_{j=1}^{J} A_{ij} x_{ij} \quad (12)$$

426 By systematically changing the weights, the optimal solutions can be found on the
427 Pareto front, which may be discrete and its shape may not be convex. An open-source
428 solver called LP_Solve was used to find five optimal solutions, respectively setting the
429 weight, w, equal to 0.1, 0.3, 0.5, 0.7, and 0.9 (Fig. 7). The five optimal solutions were
430 identical to the corresponding solutions using the *gamultiobj* function in Matlab, which
431 suggests that the results of the *gamultiobj* optimization were reliable.

432 The optimal solution with the maximum volume of transferred flood water at
433 minimum power cost was chosen (Table 4). The first part was 60 flooded area characters,
434 including floodID, the largest depth (mm), flooded area (m^2), and flood volume (m^3). The
435 second part was the optimal drain destination transferred from every flooded area.

During the drainage decision, many other issues may be considered. For example, flood at one water-logged area would be transferred simultaneously to more than one reservoir, and the priority of transferring flood water would be considered to minimize the loss of remaining flooded areas. The above drainage optimization model could be improved to meet those requirements, by adjusting variables and objectives.

$$Outflood: max \sum_{j=1}^{J} \sum_{i=0}^{I} v_{ij} \quad (13)$$

$$PowerCost: min \frac{\rho * g}{360 \sum_{j=1}^{J} \sum_{i=0}^{I} A_{ij} * v_{ij}} \quad (14)$$

$$FloodLoss: min \sum_{i=1}^{I} \sum_{k=1}^{K} (P_k * s_{ik}) \quad (15)$$

Objective (13) seeks to maximize the volume of the transferred flood water (unit: cubic meter). The output volume of the flooded area i is transferred into reservoir j (unit: cubic meter), a decision variable. Objective (14) seeks to minimize the power cost of transferring flood (unit: kWh). Objective (15) seeks to minimize the loss of flooded area according to different land use types (unit: dollar). The s_{ik} denotes the remainder of the flooded area of land use type k in flooded area i, after transferring water (unit: square meter), a decision variable. P_k is the average loss price of land use type k in flooded area i, which is a given value.

The optimization model with three objective functions is an improved version, in which some constraints can be considered, such as water-log loss. It is also practicable in urban water-log emergency decisions.

5. Conclusion

Urban water-logging is inevitable posing a significant challenge for urban drainage

458 management and emergency decision-making. This study proposes a method of integrating
459 simulation-based, urban water-logging prediction and drainage decision optimization. For
460 the fragmentation and space complexity of urban surface, urban water-logging was
461 simulated using a cellular automaton model and rules instead of mathematical runoff
462 equations. The principle of the simulation model is simple, yet powerful as it can simulate
463 uncertain flow at any position and predict water-log depth at any moment by inputting
464 DEM, land use, gully, and rainfall. This approach assumes that the urban drainage line
465 system can absorb all the down-seeping rainwater through the stormwater inlet and works
466 smoothly. The results of urban water-logging were confirmed to agree with the observed
467 outcome in two real rainfall events in the DongHaoChong basin, in the urban area of
468 Guangzhou, China. Moreover, urban water-log was predicted with a 100-year storm for
469 drainage decisions. A multi-objective optimization model for drainage decision-making
470 was proposed and applied to pumping the flood water from the predicted water-logged
471 areas to candidate reservoirs in the study area. The Pareto front was determined and tested
472 using a weighted method, from which it was simple to select an optimal drainage solution.
473 Although this model is reliable, but its precision of simulation depends on the data and
474 parameters. The optimization model, it can be improved to meet three objectives including
475 maximizing volume, minimizing the cost of transferring the flood, and minimizing the loss
476 in the remaining flooded areas. The integrated process of water-log prediction and
477 drainage optimization is useful for designing emergency plans to prevent and alleviate
478 urban water-log.
479

480 **References**

481 Asia Development Bank (ADB) (2014) Urban Stormwater Management and Waterlogging
482 Disaster Prevention. Water Supply and Other Municipal Infrastructure and Services.
483 Bach PM, Rauch W, Mikkelsen PS, McCarthy DT, Deletic A (2014) A critical review of
484 integrated urban water modelling–Urban drainage and beyond. Environ Modell Softw
485 54:88–107. https://doi.org/10.1016/j.envsoft.2013.12.018
486 Burrough PA, McDonnell RA (1998) Principles of Geographical Information Systems. Oxford
487 University Press, Oxford.
488 Cirbus J, Podhoranyi M (2013) Cellular automata for the flow simulations on the earth
489 surface, optimization computation process. Appl Math Inf Sci 7:2149–2158.
490 https://doi.org/10.12785/amis/070605
491 Deb K (2001) Multi-Objective Optimization Using Evolutionary Algorithms. John Wiley &
492 Sons, Chichester.
493 Diaz RG (2005) Analysis of Manning coefficient for small-depth flows on vegetated beds.
494 Hydrol Process 19:3221–3233. https://doi.org/10.1002/hyp.5820
495 Dong Z, Lu J (2008) Numerical simulation of urban waterlogging disaster due to Plum storm,
496 Proceedings of 16th IAHR-APD Congress and 3rd Symposium of IAHR-ISHS. Hohai
497 University, Nanjing, China.
498 Elliott AH, Trowsdale SA (2007) A review of models for low impact urban stormwater
499 drainage. Environ Modell Softw 22:394–405.
500 https://doi.org/10.1016/j.envsoft.2005.12.005
501 Ellis JB, Deutsch JC, Mouchel JM, Scholes L, Revitt MD (2004) Multicriteria decision

502 approaches to support sustainable drainage options for the treatment of highway and
503 urban runoff. Sci Total Environ 334–335:251–260.
504 https://doi.org/10.1016/j.scitotenv.2004.04.066.
505 Engineeringtoolbox (2015) Water - Dynamic and Kinematic Viscosity. (Website:
506 www.engineeringtoolbox.com/water-dynamic-kinematic-viscosity-
507 d_596.html?msclkid=7553ebffc70e11ec8243fe39d743f670)
508 Gao T (2006) Analysis on design of urban road gully. China Water & Waste Water 22:55–58.
509 García-Palomares JC, Gutiérrez J, Latorre M (2012) Optimizing the location of stations in
510 bike-sharing programs: A GIS approach. Appl Geog 35:235–246.
511 https://doi.org/10.1016/J.APGEOG.2012.07.002
512 Gu L, Gu N (2014) Urban waterlogging and stormwater management. Appl. Mech. Mater.
513 587–589:554–557. https://doi.org/10.4028/www.scientific.net/AMM.587-589.554
514 Hughes JD, Langevin CD, White, JT (2014) MODFLOW-Based Coupled Surface Water
515 Routing and Groundwater-Flow Simulation. Groundwater 53:452–463.
516 https://doi.org/10.1111/gwat.12216
517 Labadie JW, Zheng F, Wan Y (2012) Optimal integrated operation of reservoir-assisted
518 stormwater treatment areas for estuarine habitat restoration. Environment Model
519 Software 38:271–282. https://doi.org/10.1016/j.envsoft.2012.07.005
520 Liu L, Liu Y, Wang X, Yu D, Liu K, Huang H, Hu G (2014) Developing an effective 2-D
521 urban flood inundation model for city emergency management based on cellular
522 automata. Nat Hazards Earth Syst Sci 2:6173–6199. https://doi.org/10.5194/nhess-15-
523 381-2015

524 Liu N, Huang B, Pan X (2005) Using the ant algorithm to derive Pareto fronts for multi-
525 objective siting of emergency service facilities. Transp Res Rec 1935:120–129.
526 https://doi.org/10.1177/0361198105193500114
527 Ma, Ting & ZHOU, Cheng-Hu & CAI, Qiang-Guo. (2009) Modeling of hillslope runoff and
528 soil erosion at rainfall events using cellular automata approach. Pedosphere 19:711–718.
529 https://doi.org/10.1016/S1002-0160(09)60166-1.
530 Marlow DR, Moglia M, Cook S, Beale DJ (2013) Towards sustainable urban water
531 management: A critical reassessment. Water Res 47:7150–7161.
532 https://doi.org/10.1016/j.watres.2013.07.046
533 MathWorks (2012) Optimization Toolbox of Matlab. MathWorks Inc., Natick, Massachusetts
534 01760 USA.
535 Park CH, Joo JG, Kim JH (2012) Integrated washland optimization model for flood mitigation
536 using multi-objective genetic algorithm. J Hydro-Environ Res 6:119–126.
537 https://doi.org/10.1016/j.jher.2012.01.004
538 Parsons JA, Fonstad MA (2007) A cellular automata model of surface water flow. Hydrol
539 Process 21:2189–2195. https://doi.org/10.1002/hyp.6587
540 Penn R, Friedler E, Ostfeld A (2013) Multi-objective evolutionary optimization for greywater
541 reuse in municipal sewer systems. Water Res 47:5911–5920.
542 https://doi.org/10.1016/j.watres.2013.07.012
543 Quan RS, Liu M, Lu M, Zhang L, Wang J, Xu S (2010) Waterlogging risk assessment based
544 on land use cover change: A case study in Pudong New Area, Shanghai. Environ Earth
545 Sci 61:1113–1121. https://doi.org/10.1007/s12665-009-0431-8

546 Samanlioglu F (2013) A multi-objective mathematical model for the industrial hazardous
547 waste location-routing problem. Eur J Oper Res 226:332–340.
548 https://doi.org/10.1016/j.ejor.2012.11.019
549 Schaffranek RW (2004) Simulation of Surface-Water Integrated Flow and Transport in Two
550 Dimensions: SWIFT2D User's manual, in: Survey, U.S.G. (Ed.), Modeling Techniques,
551 Reston, Virginia.
552 Spitz FJ (2007) Simulation of surface water conditions in the nontidal Passaic River Basin,
553 New Jersey. https://doi.org/10.3133/sir20075052
554 Tang FP, Li MC, Qin F (2010) Distributed rainfall-runoff simulating based on cellular
555 automata for a small watershed. Adv Water Resour 21:173–178.
556 Valipour M (2014) Drainage, waterlogging and salinity. Arch Agron Soil Sci 60:1625–1640.
557 https://doi.org/10.1080/03650340.2014.905676
558 Wang FCO, Valeriano S, Sun X (2013) Near real-time optimization of multi-reservoir during
559 flood season in the Fengman basin of China. Water Resour Manage 27:4315–4335.
560 https://doi.org/10.1007/s11269-013-0410-4
561 Water Affairs Bureau, GZ (2011) Central urban rainstorm formula and calculation chart in
562 Guangzhou city, Guangzhou, pp. 3–14.
563 Woodward M, Kapelan Z, Gouldby B (2014) Adaptive flood risk management under climate
564 change uncertainty using real options and optimization. Risk Anal 34:75–92.
565 https://doi.org/10.1111/risa.12088
566 Xiao N, Bennett DA, Armstrong MP (2007) Interactive evolutionary approaches to multi-
567 objective spatial decision making: A synthetic review. Comput Environ Urban Syst

31:232–252. https://doi.org/10.1016/j.compenvurbsys.2006.08.001

Statements & Declarations

Funding: This research was partially supported by a grant from Guangzhou Major Sci-Tech project award no. 202103050001 in China.

Competing Interests: The authors have no competing interests to disclose.

Author Contributions

Conceptualization and funding, S.C. ; methodology and formal analysis, S.B.; software and validation, Z.L. and B.C.; writing—original draft preparation, Z.L.; writing—review and editing, S.B. and S.C.; visualization, B.C.. All authors have read and agreed to the published version of the manuscript.

Tables

Table 1 The computation of water depth in different covering surfaces

Ground cover type in current cell		**Calculation of water depth in current cell**	**Notation**
Permeable surface	Green land, wet land or lake	Eq. (2)	If no gully in cellular, $g(c,t) = 0$
Impermeable surface	Road, square, etc.	$I(c) = sI(c,t) = 0$ in Eq. (2)	
	Building, viaduct	$\Delta h = 0$	full discharge to sewer system

582

583 **Table 2** The list of data sources

Name	**Data type**	**Amount**	**Value type**	**Unit**	**Notation**
DEM	grid data	980*807	Double	meter	Resolution 5m
Land use	grid data	980*807	Integer		Resolution 5m 1 rep road, 2:building, 3: Greenland, 4:river or lake
gully	vector data		Geo point		With attributes of surface size, flow and block coefficient
rainfall	time series data		Double	mm	depends on rain duration
flooded areas	vector data		Geo point	cm	observed data after rainfall

584

585

586 **Table 3** The list of calibrated parameters

Name	**Data type**	**Value**	**Unit**	**Notation**
Manning coefficient	parameter	0.075		green land
		0.024		Concrete roads
		0.015		Concrete building
		0.055		Lake/river
		0.016		Asphalt viaduct
f_C	Horton para.	1.5	mm /min	permeable surface
f_0	Horton para.	16.5	mm /min	permeable surface
λ	Horton para.	1		permeable surface
I(c)	Interception	1.5	mm	permeable surface
S(c)	Sink constant	3.5	mm	permeable surface
		2	mm	impermeable surface
C	Flow coefficient	0.8		round gully
		0.6		square gully
K	Block coefficient	2/3		

587

588

589 **Table 4** The optimal solution with maximum volume and minimum energy of transferring

590 flood water

Reservoir	Capacity (m^3)	Flood ID	Depth (mm)	Area (m^2)	Volume (m^3)	Cost (kWh)
1	10500	4	2123.8149	13500	658.1	495.7
1		19	1031.6986	8950	305.1	1271.3
1		20	1019.2893	2000	79.4	139.9
1		59	241.97005	10200	80.9	130.2
2	3000	3	2241.7153	15775	373.6	743.6
2		7	1667.8442	10350	615.7	696.7
2		10	1513.9525	11200	563.8	351.8
2		14	1461.4508	1125	50.4	69.6
2		28	831.33105	2525	68.4	128.3
2		31	761.82129	4300	83.0	95.5
2		38	644.47198	3100	63.5	78.6
2		50	341.68088	4425	53.0	57.6
2		55	293.52545	6050	75.9	145.5
2		56	274.64941	6675	77.1	106.3
3	6300	40	629.70514	4650	127.5	209.0
3		46	468.60483	3900	62.6	52.3
3		48	416.48105	3850	62.9	86.5
3		53	309.09201	8450	84.8	169.3
4	3000	5	2121.3005	24275	1427.8	1661.9

4		16	1323.0109	1425	62.5	80.1
4		30	765.13538	7225	267.3	155.1
4		39	631.7746	5025	79.0	114.0
4		51	339.31653	2825	51.3	38.7
4		60	238.77893	6275	62.4	102.4
5	35000	6	1821.7334	2725	151.5	346.9
5		12	1498.4288	2275	86.2	64.0
5		23	998.95313	10225	170.3	518.1
5		25	920.39471	7350	246.1	253.7
5		26	861.73035	1400	52.1	22.5
5		29	819.4292	15825	510.5	1140.6
5		33	757.79053	4825	72.9	142.4
5		34	745.80585	59650	1049.5	203.0
5		36	699.97461	21050	337.7	432.4
5		41	609.38672	14575	307.5	815.7
5		42	567.39093	19925	307.4	576.7
5		43	544.59082	3300	64.0	130.2
5		52	334.93088	7675	94.3	308.3
5		54	300.30109	4625	62.0	108.2
6	10000	15	1453.9644	7900	398.5	861.0
6		17	1144.4536	4225	166.7	335.1
6		24	920.51135	1575	75.0	136.3

6		35	703.53833	4150	86.0	203.8
6		37	679.5484	4050	95.2	128.9
6		45	486.42014	23800	316.6	40.5
6		47	437.69373	9400	152.9	69.4
6		49	365.22165	11050	107.3	250.0
6		57	260.64087	11425	115.7	213.7
6		58	246.61449	7650	76.6	52.5
7	50000	1	2908.5427	4200	423.0	356.8
7		2	2458.1958	91350	3622.0	10484.9
7		8	1659.0315	12300	443.8	6.2
7		9	1656.8096	14000	840.1	1149.3
7		11	1500.2119	7125	344.3	333.9
7		13	1479.0426	10150	520.3	516.9
7		21	1018.4205	4325	197.9	366.3
7		22	1014.3046	4025	154.3	143.9
7		32	761.09271	4150	110.5	142.2
7		44	496.6109	52550	1540.0	4175.4
8	6700	18	1076.0411	50200	1103.5	1301.5
8		27	850.0863	1700	63.8	143.7

591

592

593 **Figure legends**

594 **Fig. 1** Study area of DongHaoChong basin in urban Guangzhou. (**a**) Study area is in the
595 urban area of Guangzhou city in GuangDong province. (**b**) DongHaoChong basin is a part
596 of the Pearl River basin

597

598 **Fig. 2** Main process of simulating water-log

599

600 **Fig. 3** Comparison of simulated and observed depth in main water-logging areas. (**a**) 15
601 August, 2013 (**b**) 23 June, 2014

602

603 **Fig. 4** Water-log depth map simulated by cellular automata (CA) with predicted storms.
604 **(a)** Water-log depth map simulated by CA with 1-year-storm. (**b)** Water-log depth map
605 simulated by CA with 10-year-storm. **(c)** Water-log depth map simulated by CA with 50-
606 year-storm. **(d)** Water-log depth map simulated by CA with 100-year-storm

607

608 **Fig. 5** Predicted flooded areas in a 100-year storm and the reservoir statuses

609

610 **Fig. 6** Pareto front of multi-objective optimization based on genetic algorithms

611

612 **Fig. 7** Results of single objective optimization using the weighted method

613

Figures

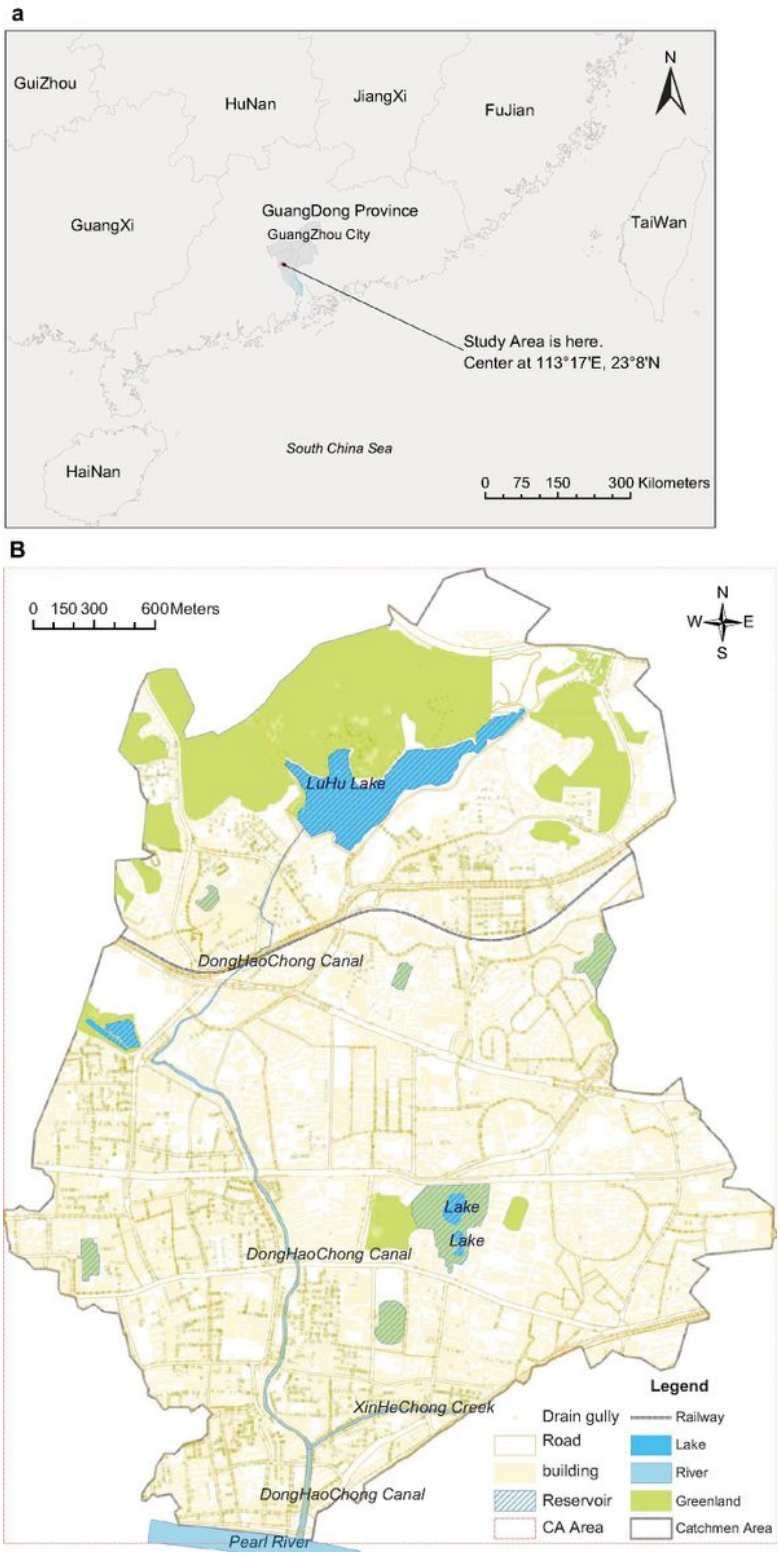

Figure 1

Study area of DongHaoChong basin in urban Guangzhou. (**a**) Study area is in the urban area of Guangzhou city in GuangDong province. (**b**) DongHaoChong basin is a part of the Pearl River basin

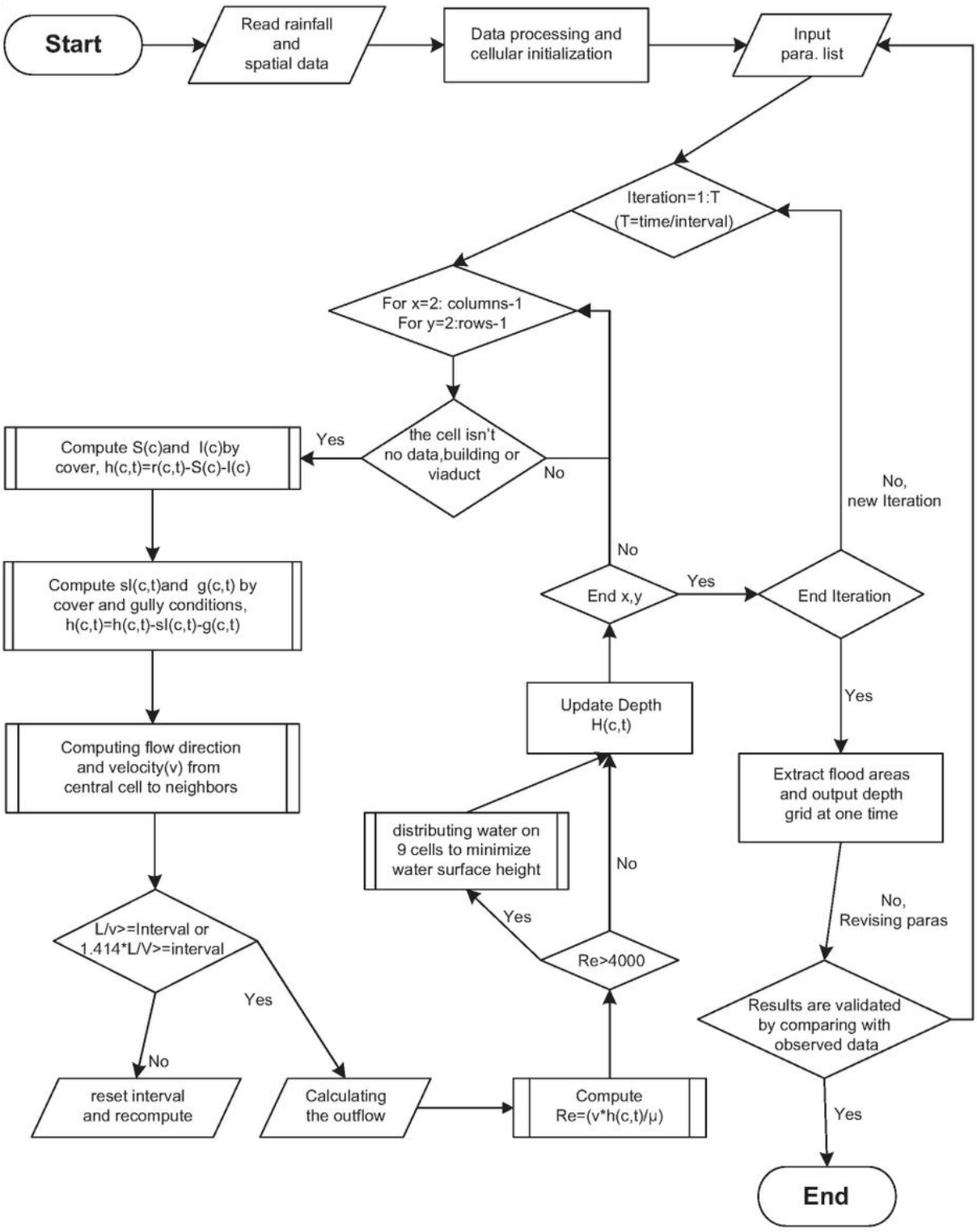

Figure 2

Main process of simulating water-log

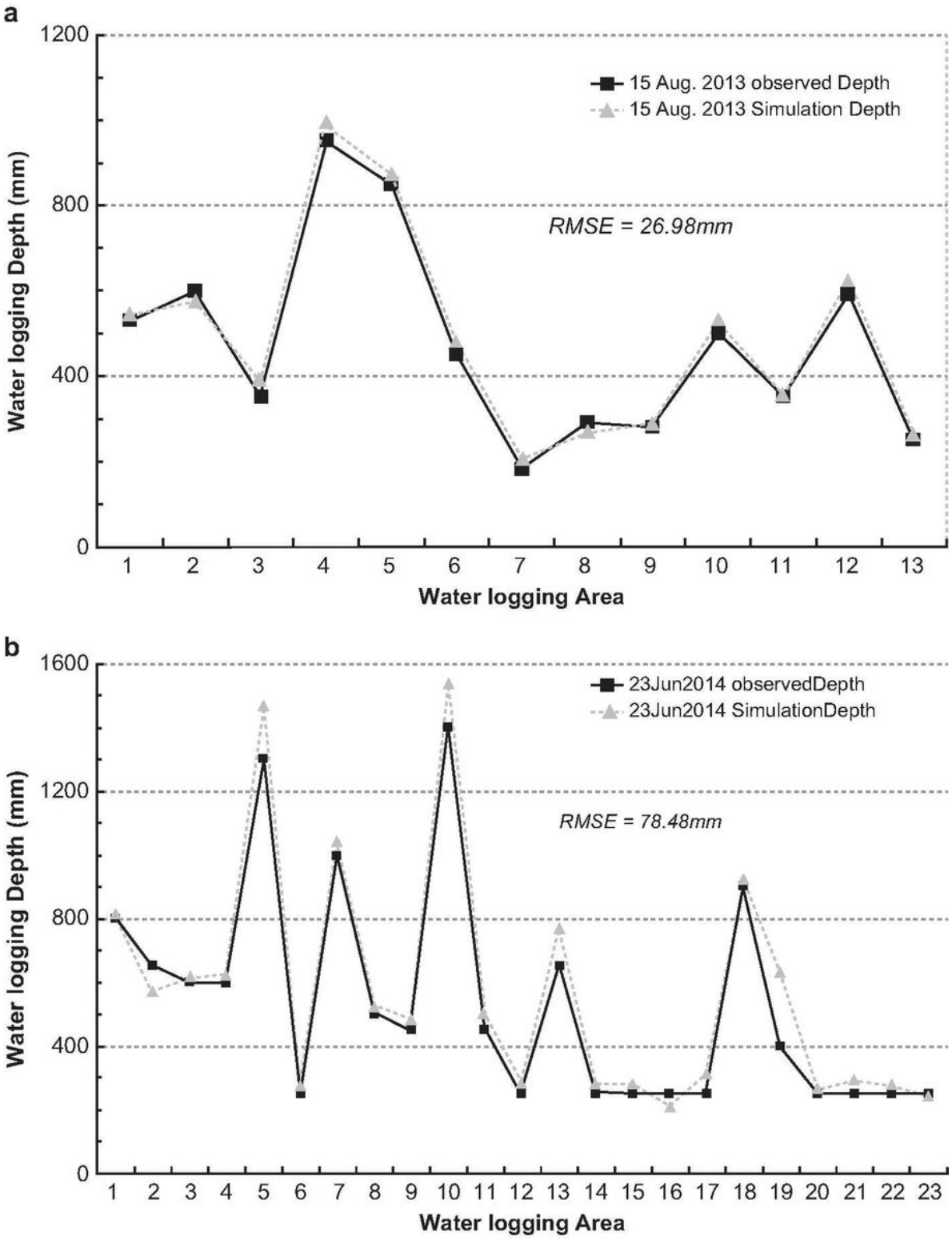

Figure 3

Comparison of simulated and observed depth in main water-logging areas. (**a**) 15 August, 2013 (**b**) 23 June, 2014

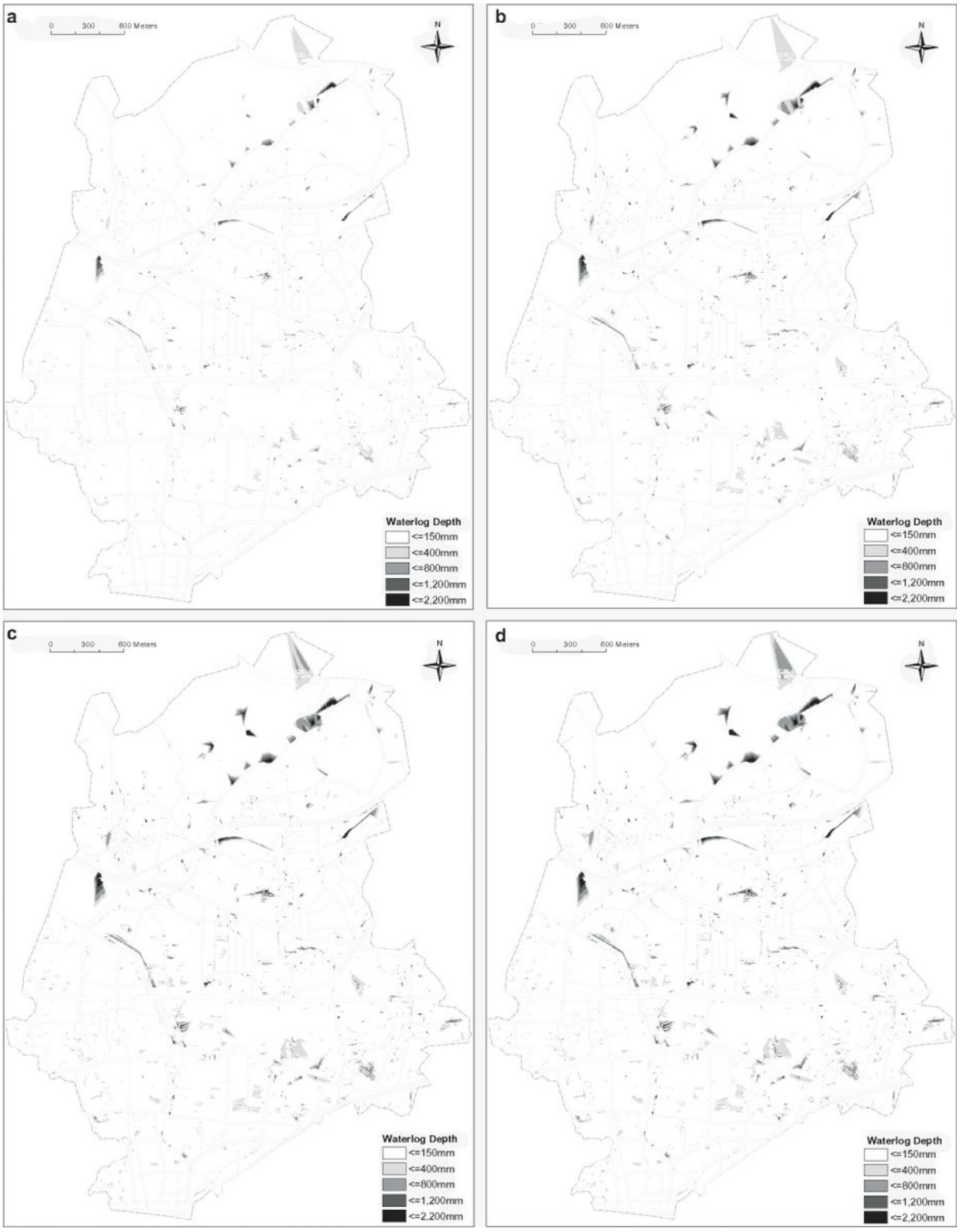

Figure 4

Water-log depth map simulated by cellular automata (CA) with predicted storms. **(a)** Water-log depth map simulated by CA with 1-year-storm. (**b)** Water-log depth map simulated by CA with 10-year-storm. **(c)** Water-log depth map simulated by CA with 50-year-storm. **(d)** Water-log depth map simulated by CA with 100-year-storm

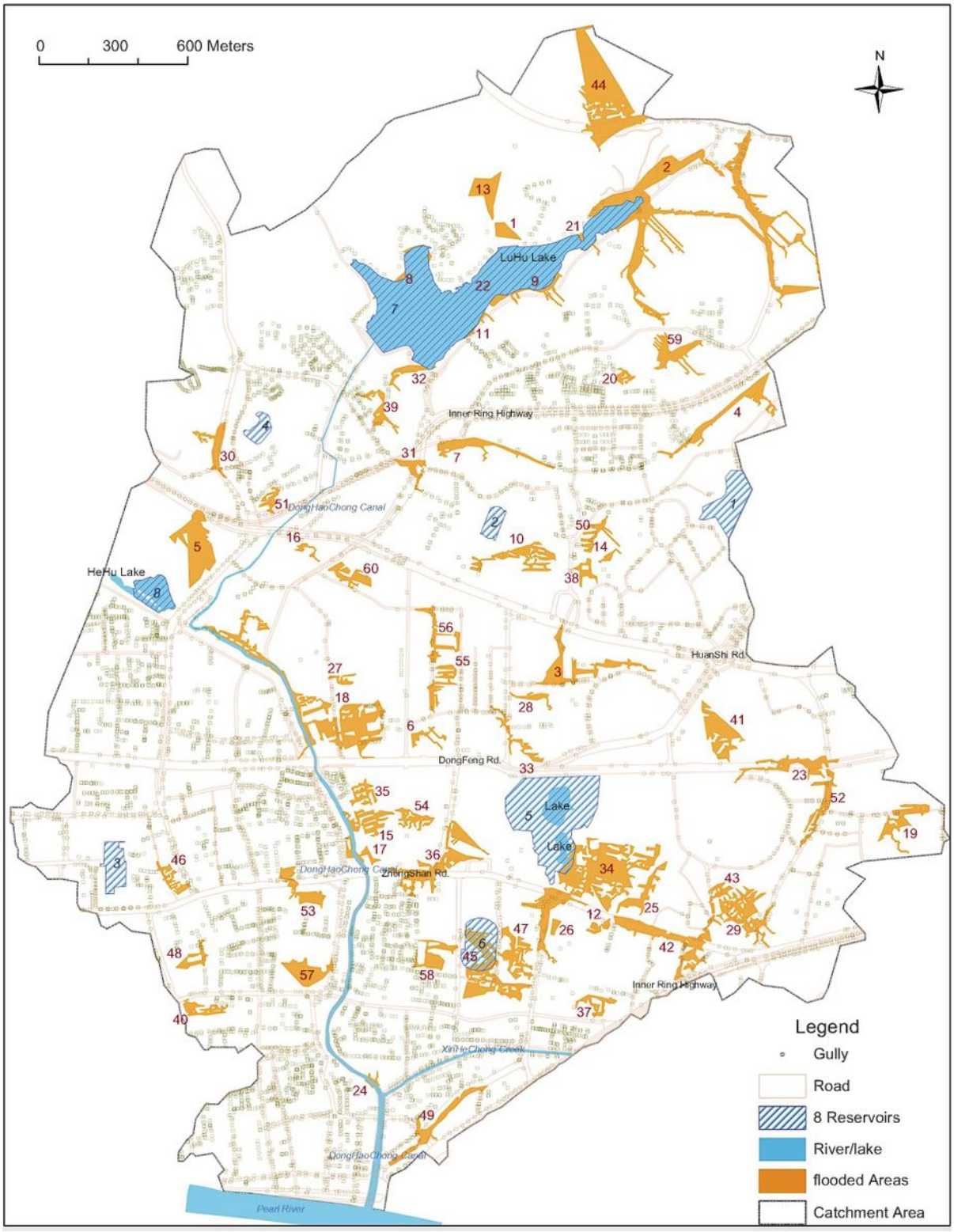

Figure 5

Predicted flooded areas in a 100-year storm and the reservoir statuses

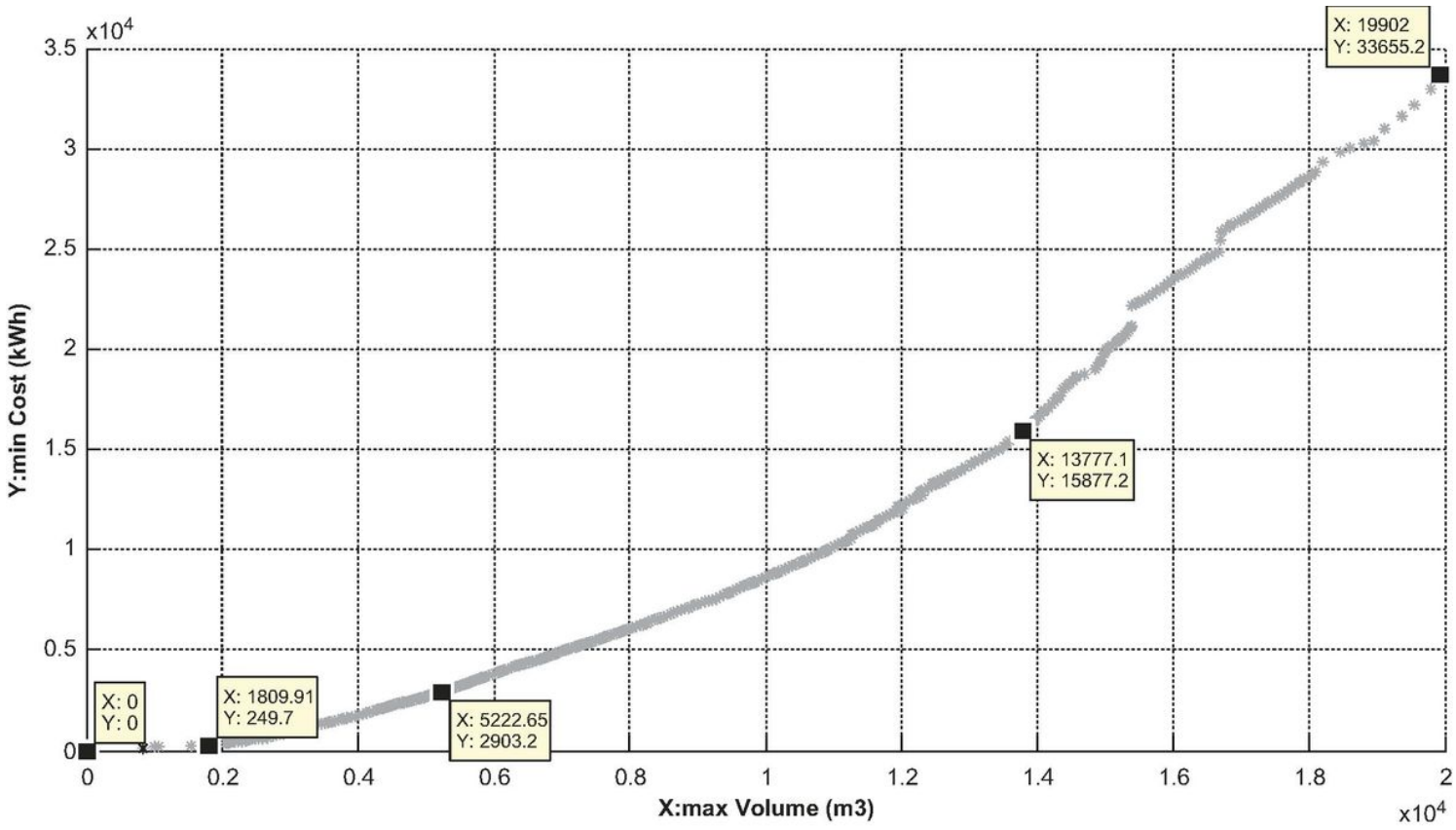

Figure 6

Pareto front of multi-objective optimization based on genetic algorithms

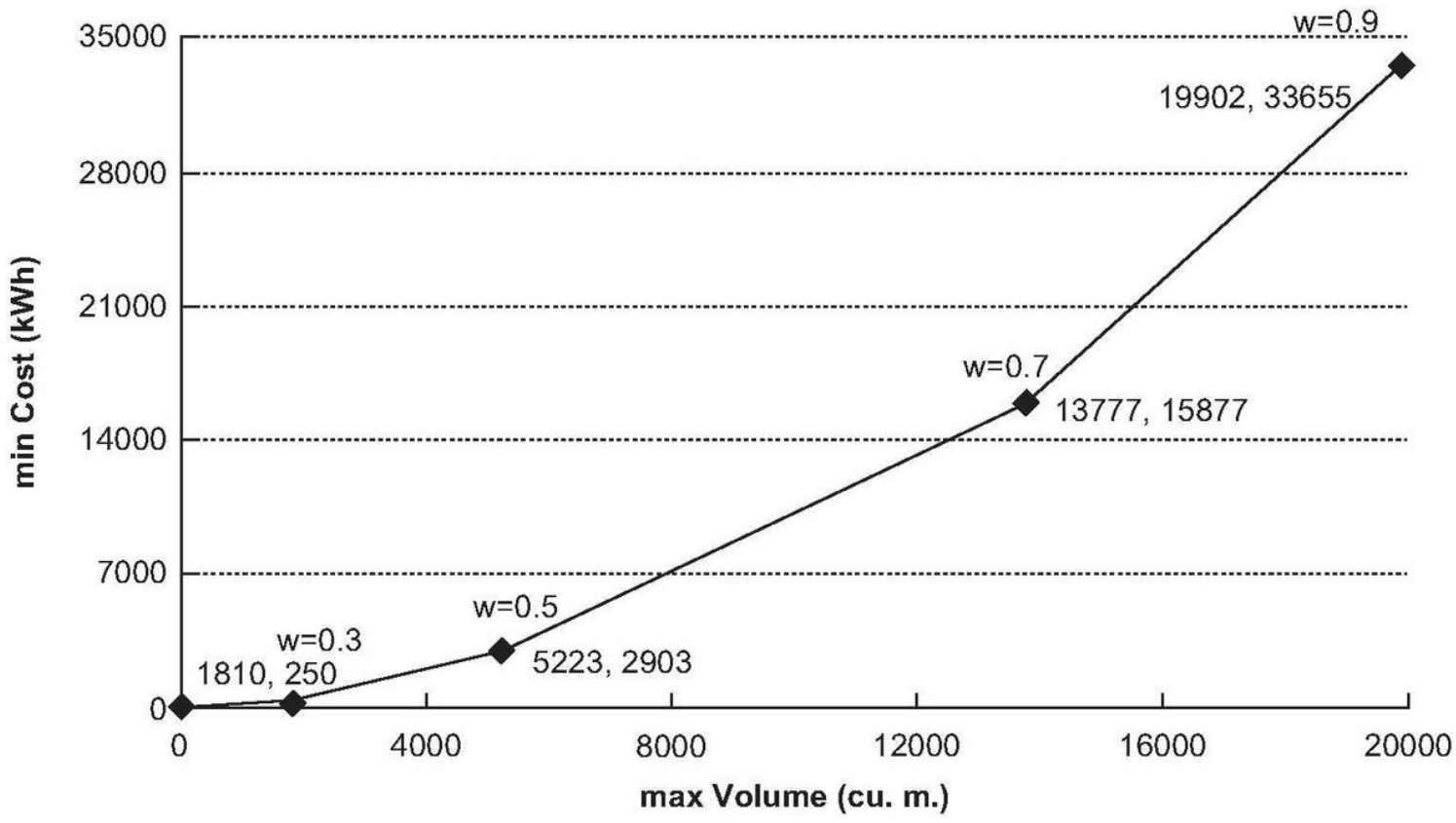

Figure 7

Results of single objective optimization using the weighted method